Macromolecules

pubs.acs.org/Macromolecules Article

Temperature-Dependent Ring-Opening Polymerization-Induced Self-Assembly Using Crystallizable Polylactones as Core-Forming Blocks

Ding Shen, Boyang Shi, Peng Zhou, Di Li, and Guowei Wang*

Cite This: *Macromolecules* 2023, 56, 4814–4822 Read Online

ACCESS | Metrics & More | Article Recommendations | Supporting Information

ABSTRACT: Ring-opening polymerization-induced self-assembly (ROPISA) was achieved by employing hydroxyl-terminated polyisobutylene (PIB-OH), diphenyl phosphate (DPP), cyclohexane, and ε-caprolactone (ε-CL) and/or δ-valerolactone (δ-VL) as the stabilizer/macroinitiator, catalyst, solvent, and monomers, respectively. ROPISA has enabled the introduction of biodegradable, biocompatible, and crystallizable polylactones to nanoparticles and related materials. The polymerization temperatures (20, 50, or 80 °C) had an important effect on the crystallization behavior and corresponding self-assembly of PIB-*b*-PCL and PIB-*b*-PVL. The highest temperature (80 °C) interfered with the crystallization and *in situ* fixation, which readily reorganized nanoparticles and formed either spherical micelles or a precipitate. However, at the lowest temperature (20 °C), fibrillar nanoparticles were gradually formed and stabilized according to the classical polymerization-induced self-assembly (PISA) mechanism. Furthermore, temperature adjustment altered the monomer sequence in the P(CL-*co*-VL) block and the subsequent crystallization and self-assembly. At 80 °C, the P(CL-*co*-VL) block formed a weakly crystallized random structure, which generated spherical micelles. By contrast, at 20 °C, ROPISA favored the generation of P(CL-*co*-VL) containing a quasi-block sequence, resulting in the acquisition of fibrillar micelles. Interestingly, at different polymerization temperatures, nanoparticles exhibited different morphologies, even when the compositions were similar. The results of this study revealed that ROPISA provided a feasible alternative to PISA for synthesizing nanoparticles.

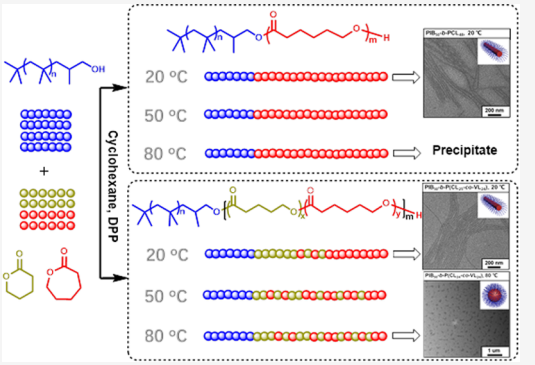

INTRODUCTION

Polylactones are sustainable, biocompatible, and biodegradable polymers, which can be synthesized *via* ring-opening polymerization (ROP).[1,2] For polylactones, ROP has been extensively studied and is characterized by a high monomer conversion, tolerance for various solvents, and mild polymerization conditions.[3−7] The most-studied lactone monomers are ε-caprolactone (ε-CL), δ-valerolactone (δ-VL), trimethylene carbonate (TMC), and L-lactide (LLA).[8−10] Traditionally, polylactones have been mostly introduced to block copolymers, and their self-assemblies are preferred in certain applications. For example, micelles containing a poly(L-lactic acid) (PLLA) core-forming block have been studied by Han et al.[11] and O'Reilly et al.,[12−14] and micelles containing a poly(ε-caprolactone) (PCL) core-forming block have been investigated by Xu et al.,[15,16] Eisenberg et al.,[17−19] and Discher et al.[20] All of these micelles have potential drug delivery applications, specifically for delivering the anticancer drug paclitaxel.[21] However, these micelles are typically prepared *via* conventional self-assembly by transferring a block copolymer solution to a selective solvent at relatively low concentrations (<1.0% w/w), and the synthesis methods feature limited scalability and complex procedures. Consequently, these drawbacks ultimately limit the practical application of micelles.[22]

Alternatively, the recently developed polymerization-induced self-assembly (PISA) technique can be used for easily synthesizing a wide variety of micellar morphologies at relatively high solids (up to 50% w/w).[23−28] Additionally, PISA has been extensively used for multiple applications.[29−34] However, core-forming blocks are noncrystallizable in the most-studied PISA system, in which the driving force for self-assembly is the solubility change of the core-forming blocks. When a crystallizable block is introduced to PISA, crystallization functions as an alternative driving force, which dominates the formation of different micellar morphologies.[35,36] Thus, ring-opening polymerization-induced self-assembly (ROPISA) was investigated for lactone monomers. For example, Patterson et al.[37] used ROPISA for the LLA

Received: April 12, 2023
Revised: June 10, 2023
Published: June 23, 2023

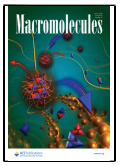

https://doi.org/10.1021/acs.macromol.3c00681
Macromolecules 2023, 56, 4814−4822

Scheme 1. Schematic of ROPISA Using PIB-OH as the Stabilizer/Macroinitiator and PCL, PVL, or P(CL-*co*-VL) as the Core-Forming Blocks

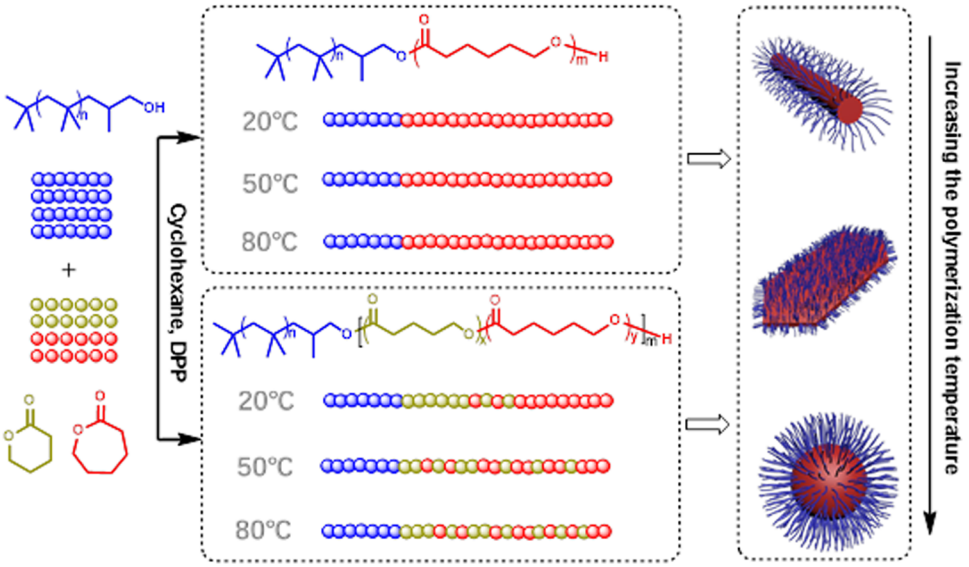

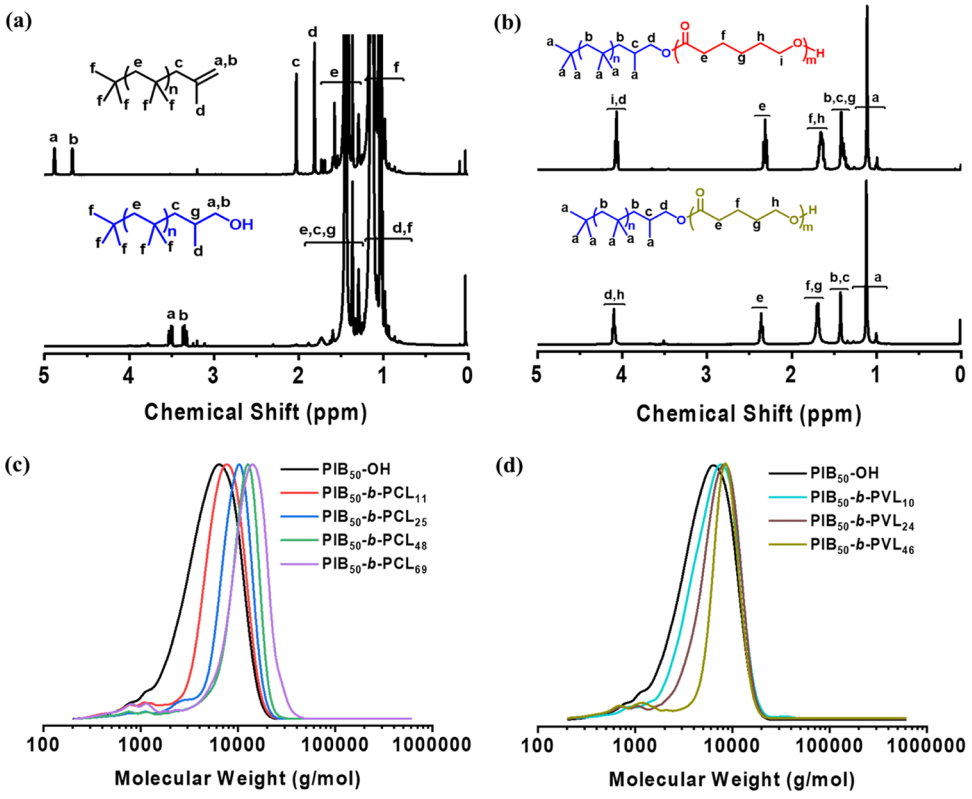

Figure 1. ^{1}H NMR spectra for (a) HRPIB and PIB_{50}-OH (in $CDCl_3$) and (b) PIB_{50}-*b*-PCL_{48} and PIB_{50}-*b*-PVL_{46} (in $CDCl_3$). (c, d) GPC curves for PIB_{50}-*b*-PCL_x and PIB_{50}-*b*-PVL_x block copolymers (dissolved in THF eluent), where *x* represents DP.

monomer, which targeted the PLLA-*b*-poly(ethylene glycol) (PLLA-*b*-PEG) diblock copolymer. Du et al.[38] and Bonduelle et al.[39,40] used ROPISA and the amine-terminated polyethylene glycol ($PEG-NH_2$) macroinitiator for the *N*-carboxyanhydride (NCA) monomer. Yang et al.[41] used ROPISA and the hydroxyl-terminated polyethylene glycol (PEG-OH) macroinitiator for the salicylic acid *o*-carboxyanhydride (SAOCA) monomer. Alternatively, Manners et al.[42] investigated ROPISA for a poly(fluorenetrimethylenecarbonate) (PFTMC) core and a hydrophilic polyethylene glycol (PEG) corona. Spheres, rods, fibers, lamellae, and stacked lamellae can all be obtained *via* ROPISA, which provided an alternative method for synthesizing novel biodegradable nanoparticles.[43]

Importantly, however, because the crystallization is always temperature-dependent, the polymerization temperature should considerably affect the crystallization behavior of the crystallizable core-forming block during ROPISA. Therefore,

https://doi.org/10.1021/acs.macromol.3c00681
Macromolecules 2023, 56, 4814−4822

Table 1. Formulation, Characterization, and Morphologies of Nanoparticles Obtained Using ROPISA[a]

entry	samples[b]	$[PIB_{50}\text{-}OH]_0/[\varepsilon\text{-}CL]_0/[\delta\text{-}VL]_0$	temperature (°C)	conversion (%, ε-CL/δ-VL)[c]	$M_{n,GPC}$ (g/mol)[d]	M_w/M_n[d]	morphologies[e]
1	PIB_{50}-*b*-PCL_{11}	1/12/0	20	100/0	5900	1.22	fiber and sphere
2	PIB_{50}-*b*-PCL_{11}	1/12/0	50	100/0	5900	1.21	short fiber and platelet
3	PIB_{50}-*b*-PCL_{10}	1/12/0	80	98/0	5800	1.25	sphere
4	PIB_{50}-*b*-PCL_{25}	1/24/0	20	99/0	7400	1.29	fiber
5	PIB_{50}-*b*-PCL_{24}	1/24/0	50	99/0	6900	1.21	sphere with platelet
6	PIB_{50}-*b*-PCL_{27}	1/24/0	80	98/0	6400	1.24	sphere with fusiform platelet
7	PIB_{50}-*b*-PCL_{48}	1/48/0	20	96/0	9500	1.22	fiber
8	PIB_{50}-*b*-PCL_{49}	1/48/0	50	98/0	9300	1.18	precipitate
9	PIB_{50}-*b*-PCL_{49}	1/48/0	80	99/0	9900	1.20	precipitate
10	PIB_{50}-*b*-PCL_{69}	1/72/0	20	95/0	11,800	1.18	precipitate
11	PIB_{50}-*b*-PVL_{10}	1/0/12	20	0/100	5200	1.26	fiber with irregular structure
12	PIB_{50}-*b*-PVL_{24}	1/0/24	20	0/94	6200	1.28	precipitate
13	PIB_{50}-*b*-PVL_{46}	1/0/48	20	0/98	8300	1.08	precipitate
14	PIB_{50}-*b*-P(CL_{25}-*co*-VL_{24})	1/24/24	20	100/100	9100	1.12	fiber
15	PIB_{50}-*b*-P(CL_{24}-*co*-VL_{25})	1/24/24	50	100/100	9200	1.21	sphere
16	PIB_{50}-*b*-P(CL_{24}-*co*-VL_{24})	1/24/24	80	98/97	9000	1.22	sphere

[a]PIB_{50}-OH ($M_{n,GPC}$ = 2800 g/mol), DPP, and cyclohexane were used as the stabilizer/macroinitiator, catalyst, and solvent, respectively, and solids were 10% w/w. [b]Subscript represents DP for each block, which was calculated based on ^{1}H NMR spectra. [c]Monomer conversion was calculated based on ^{1}H NMR spectra. [d]$M_{n,GPC}$ and M_w/M_n were determined by GPC, wherein tetrahydrofuran (THF) and polystyrene (PS) were used as eluent and standard, respectively. [e]Morphologies were measured by transmission electron microscopy (TEM).

the self-assembly might be modulated. To the best of our knowledge, the effect of the polymerization temperature on the self-assembly has hardly been studied for ROPISA. Additionally, the PEG block has always been employed as the stabilizer/macroinitiator, which considerably limits the potential application of nanoparticles generated using ROPISA. Therefore, the investigation of ROPISA using an alternative stabilizer/macroinitiator is important in both theory and practice. Although classified as a polyolefin, polyisobutylene (PIB) is highly regarded for its exceptional thermo-oxidative stability, strong chemical resistance, and impermeability.[44] Owing to these remarkable properties, PIB-based materials have been widely applied to lubricant additives,[45,46] thermoplastic elastomers,[47,48] and pressure-sensitive adhesives.[49] Furthermore, because chemically inert repeating units on PIB can prevent the enzymatic degradation and attacks by the immune system,[50] PIB-based materials also exhibit both excellent biocompatibility and biostability and are, thus, widely used in biomedical research.[51−56]

Because of its progress and limitations, ROPISA is evidently still in its infancy, and further development is urgently required. Additionally, owing to their individual advantages, the combination of polylactone and PIB presents an opportunity to develop biodegradable or biocompatible nanomaterials. Therefore, in this study, ROPISA was re-evaluated and investigated using hydroxyl-functionalized PIB (PIB-OH), diphenyl phosphate (DPP), cyclohexane, and ε-CL and δ-VL as the stabilizer/macroinitiator, catalyst, solvent, and monomers, respectively (Scheme 1). The effects of the core-forming blocks (PCL, PVL, and P(CL-*co*-VL)) and polymerization temperatures on the morphological evolution during ROPISA were investigated and compared. The polymerization temperature showed important effects on the copolymerization kinetics, monomer sequence, crystallization behavior, and final self-assembly.

RESULTS AND DISCUSSION

PIB-*b*-PCL and PIB-*b*-PVL Block Copolymers Synthesized Using ROPISA. First, the PIB_{50}-OH ($M_{n,GPC}$ = 2800 g/mol obtained by gel permeation chromatography (GPC); molecular weight distribution (M_w/M_n) = 1.82; degree of polymerization (DP) = 50) stabilizer/macroinitiator was synthesized *via* hydroboration−oxidation of highly reactive polyisobutylene (HRPIB),[57,58] which has 83.3% terminal *exo*-olefin group content (Scheme S1, Figures S1 and 1a). As shown in the proton nuclear magnetic resonance (^{1}H NMR) spectra in Figure 1a, the resonance signals at 4.88 and 4.67 ppm were attributed to the protons bonded to the carbon atom in the terminal double bond (−C═CH_2) in HRPIB. After hydroboration−oxidation, these signals completely disappeared and resonance signals attributed to the methylene protons (−CH_2OH) appeared at 3.55 and 3.34 ppm, and the hydroxyl group was deduced to be 83.3%. This was the same as the content of the terminal *exo*-olefin group, as indicated by the ^{1}H NMR spectra.

Subsequently, PIB-*b*-PCL and PIB-*b*-PVL diblock copolymers were generated using PIB_{50}-OH, DPP, and cyclohexane as the stabilizer/macroinitiator, catalyst, and solvent for ROP of ε-CL and δ-VL monomers, respectively. Because cyclohexane was both a good solvent for the PIB block and a poor solvent for the PCL or PVL block, ROPISA was achieved. ^{1}H NMR spectra were generated to confirm that PIB-*b*-PCL and PIB-*b*-PVL diblock copolymers were synthesized by ROPISA (Figure 1b). Additionally, ROPISA was confirmed by GPC because the chromatograms exhibited a monomodal peak, controlled molecular weight (MW), and narrow M_w/M_n (Figure 1c,d).

During ROPISA, the polymerization temperature considerably affects the polymerization kinetics, crystallization behavior, and self-assembly. Therefore, in this study, polymerization temperatures of 20, 50, and 80 °C were chosen because they are either below or above the melting temperature (T_m) and crystallization temperature (T_c) of the PCL and PVL

https://doi.org/10.1021/acs.macromol.3c00681
Macromolecules 2023, 56, 4814−4822

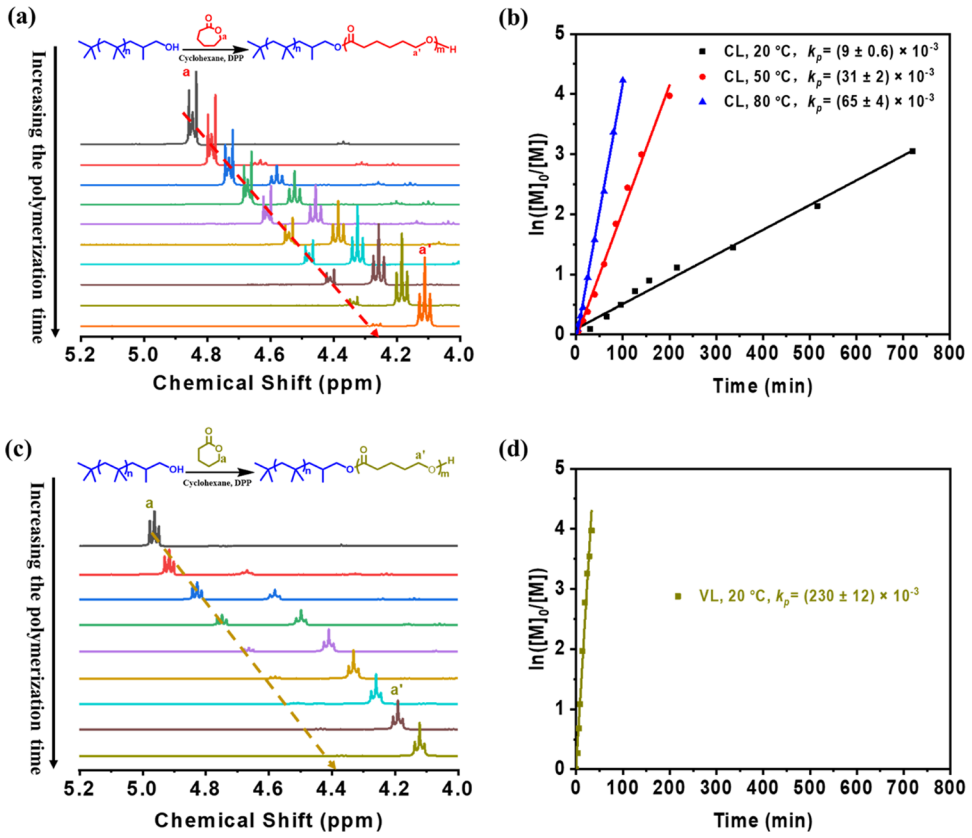

Figure 2. Polymerization kinetics for ROPISA using ε-CL or δ-VL (10% w/w solids): (a) ^{1}H NMR spectra measured at different polymerization times (in $CDCl_3$, targeted at PIB_{50}-*b*-PCL_{48} at 20 °C); (b) plots of ln([M]$_0$/[M]) *versus* time (targeted at PIB_{50}-*b*-PCL_{48} at 20 °C, PIB_{50}-*b*-PCL_{49} at 50 °C, and PIB_{50}-*b*-PCL_{49} at 80 °C); (c) ^{1}H NMR spectra measured at different polymerization times (in $CDCl_3$, targeted at PIB_{50}-*b*-PVL_{46} at 20 °C); (d) plot of ln([M]$_0$/[M]) *versus* time (targeted at PIB_{50}-*b*-PVL_{46} at 20 °C). Units for polymerization rate constants (k_p) are L·mol^{-1}·s^{-1}.

blocks. For instance, when the PIB_{50}-*b*-PCL_{48} block copolymer was synthesized at 20 °C (entry 7 in Table 1), the MW of the block copolymers regularly increased with prolonged polymerization time (Figure S2a,b). The monomer conversion was derived based on the change in the resonance signal at 4.25 ppm in the ^{1}H NMR spectra (Figure 2a). The monomers were polymerized in a living/controlled manner at a relatively high polymerization rate (Figure S2c). As shown in Figure 2b, a linear relationship was established between ln([M]$_0$/[M]) and time, and the polymerization rate constant (k_p) was calculated at (9 ± 0.6) × 10^{-3} L·mol^{-1}·s^{-1}. Similarly, at 50 and 80 °C, k_p was calculated at (31 ± 2) and (65 ± 4) × 10^{-3} L·mol^{-1}·s^{-1}, respectively (entries 8 and 9 in Table 1, Figures 2b, S3 and S4). At 20 °C, the synthesis of the PIB_{50}-*b*-PVL_{46} block copolymer (entry 13 in Table 1) was also monitored using ^{1}H NMR spectra (Figure 2c) and GPC measurements (Figure S5), and k_p was calculated at (230 ± 12) × 10^{-3} L·mol^{-1}·s^{-1} (Figure 2d). Obviously, the highest polymerization temperature (80 °C) contributed to the fastest polymerization rate and, thus, the highest k_p. Notably, at 20 °C, the δ-VL monomer showed a higher reactivity than the ε-CL monomer.

PIB-*b*-P(CL-*co*-VL) Block Copolymer Synthesized Using ROPISA. For copolymerization, the monomer sequence might affect both the crystallization and self-assembly during ROPISA. Correspondingly, the monomer sequence was modulated by adjusting the monomer reactivity ratio, which was predominantly affected by the temperature. Thus, the ε-CL and δ-VL monomers were also copolymerized at different temperatures (*i.e.*, 20, 50, and 80 °C). GPC revealed that ROPISA synthesized PIB-*b*-P(CL-*co*-VL) block copolymers exhibiting a controlled MW and narrow M_w/M_n (Figures S6–8a,b). The monomer conversion and k_p were determined using ^{1}H NMR spectra (Figure 3a). As shown in Figure 3b, at different polymerization temperatures, the ε-CL and δ-VL monomers exhibited distinct polymerization rates. At 20 °C, k_p was calculated at (14 ± 1) and (125 ± 8) × 10^{-3} L·mol^{-1}·s^{-1} for ε-CL and δ-VL, and the corresponding monomer conversion of ε-CL was only 12% when that of δ-VL reached 95% (Figure S6c). Moreover, the synthesized P(CL-*co*-VL) resembled the PVL-*b*-PCL diblock copolymer. At 50 °C, k_p was calculated at (27 ± 2) and (230 ± 6) × 10^{-3} L·mol^{-1}·s^{-1} for ε-CL and δ-VL, respectively, and the corresponding monomer conversion of ε-CL was increased to 29% when that of δ-VL reached 95% (Figure S7c). At 80 °C, k_p was calculated at (81 ± 5) and (324 ± 23) × 10^{-3} L·mol^{-1}·s^{-1} for ε-CL and δ-VL, respectively, and the corresponding monomer conversion of ε-CL was further increased to 69% when that of δ-VL reached 95% (Figure S8c). Moreover, the synthesized P(CL-*co*-VL) contained a random monomer sequence. Thus, the highest and lowest polymerization temperatures (80 and 20 °C) contributed to the formation of the random structure and facilitated the formation of the quasi-block sequence, respectively.

Crystallization Behavior of Block Copolymers Synthesized Using ROPISA. The block copolymer structures were characterized using DSC measurements. As shown in Figure 3c,d, for the PIB_{50}-*b*-PCL_{25} and PIB_{50}-*b*-PVL_{24} block copolymers, T_m and T_c were 56 and 38, 53 and 37 °C,

https://doi.org/10.1021/acs.macromol.3c00681
Macromolecules 2023, 56, 4814−4822

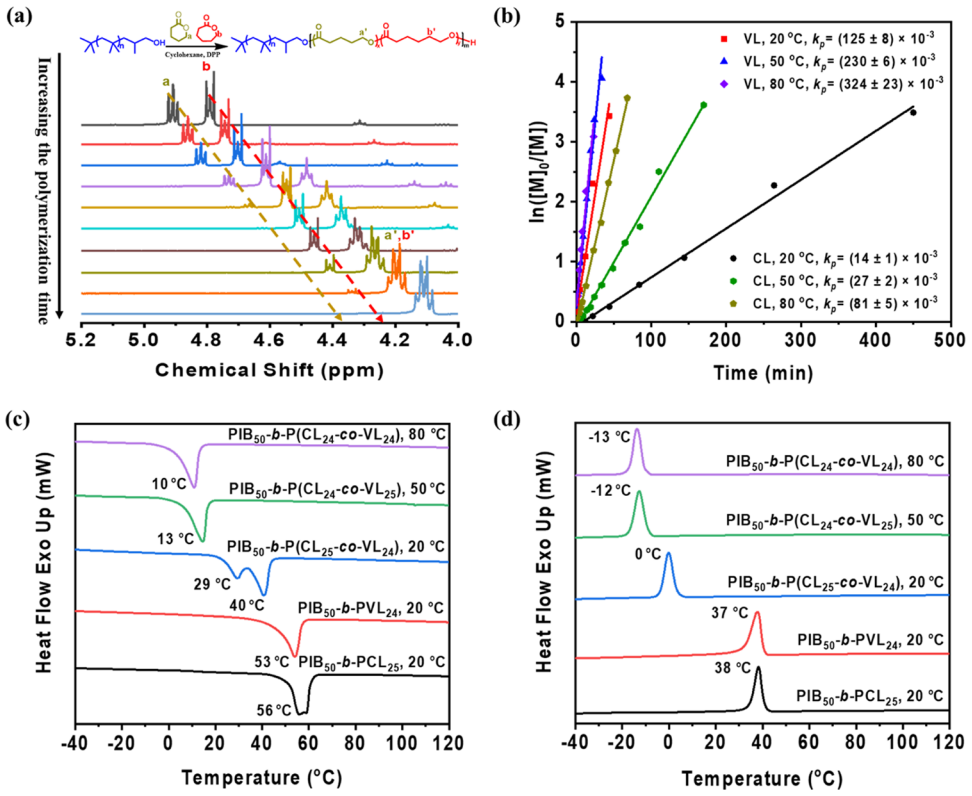

Figure 3. Polymerization kinetics for ROPISA of ε-CL and δ-VL (10% w/w solids): (a) ^{1}H NMR spectra measured at different polymerization times (in $CDCl_3$, targeted at PIB$_{50}$-*b*-P(CL$_{25}$-*co*-VL$_{24}$) at 20 °C); (b) plots of ln([M]$_0$/[M]) *versus* time (targeted at PIB$_{50}$-*b*-P(CL$_{25}$-*co*-VL$_{24}$) at 20 °C, PIB$_{50}$-*b*-P(CL$_{24}$-*co*-VL$_{25}$) at 50 °C, and PIB$_{50}$-*b*-P(CL$_{24}$-*co*-VL$_{24}$) at 80 °C); (c, d) differential scanning calorimetry (DSC) thermograms for block copolymers synthesized using different monomers at different polymerization temperatures. Units of polymerization rate constants (k_p) are L·mol^{-1}·s^{-1}.

respectively, which were consistent with T_m and T_c values published in previous studies.[59−62] Notably, for PIB$_{50}$-*b*-P(CL$_{25}$-*co*-VL$_{24}$), PIB$_{50}$-*b*-P(CL$_{24}$-*co*-VL$_{25}$), and PIB$_{50}$-*b*-P-(CL$_{24}$-*co*-VL$_{24}$), T_m and T_c both regularly decreased with increasing polymerization temperature from 20 to 50 and 80 °C. Obviously, although these copolymers had similar compositions, the copolymers had different T_m and T_c values probably because the corresponding P(CL-*co*-VL) segments contained different monomer sequences. At 80 and 20 °C, the synthesized P(CL-*co*-VL) segments exhibited random and quasi-block structures, respectively. DSC measurements further confirmed the formation of different P(CL-*co*-VL) segments at different polymerization temperatures, which was consistent with the polymerization kinetics.

Morphological Evolution of PIB-*b*-PCL and PIB-*b*-PVL during ROPISA. The morphologies of the PIB-*b*-PCL diblock copolymer nanoparticles were investigated by fixing the solids at 10% w/w while varying the PCL block length and polymerization temperature. To exclude the effect of the stirring rate on ROPISA, the stirring rate was fixed at 500 rpm during the entire polymerization and cooling process, except for the additional condition described in the next section. As shown in Figure 4a (entry 1 in Table 1), at 20 °C, the PIB$_{50}$-*b*-PCL$_{12}$ diblock copolymer was synthesized when the [PIB$_{50}$-OH]$_0$/[ε-CL]$_0$ molar ratio was 1/12, and fibrillar micelles were predominantly formed with a few spherical micelles. When [PIB$_{50}$-OH]$_0$/[ε-CL]$_0$ was increased to 1/24 and 1/48, PIB$_{50}$-*b*-PCL$_{25}$ and PIB$_{50}$-*b*-PCL$_{48}$ diblock copolymers comprising pure fibrillar micelles were synthesized, respectively (Figure 4b,c, entries 4 and 7 in Table 1). However, when [PIB$_{50}$-OH]$_0$/[ε-CL]$_0$ was further increased to 1/72, the PIB$_{50}$-*b*-PCL$_{69}$ diblock copolymer precipitated (entry 10 in Table 1).

At 50 °C and [PIB$_{50}$-OH]$_0$/[ε-CL]$_0$ = 1/12, the PIB$_{50}$-*b*-PCL$_{11}$ diblock copolymer, which comprised short fibrillar and plate-like micelles, was synthesized (Figure 4d, entry 2 in Table 1). At [PIB$_{50}$-OH]$_0$/[ε-CL]$_0$ = 1/24, the PIB$_{50}$-*b*-PCL$_{24}$ diblock copolymer, which exhibited a plate-like morphology and spherical micelles, was synthesized (Figure 4e, entry 5 in Table 1). However, when [PIB$_{50}$-OH]$_0$/[ε-CL]$_0$ was increased to 1/48, the PIB$_{50}$-*b*-PCL$_{49}$ diblock copolymer precipitated (Figure 4f, entry 8 in Table 1). Furthermore, when the polymerization temperature was increased to 80 °C and [PIB$_{50}$-OH]$_0$/[ε-CL]$_0$ = 1/12, the PIB$_{50}$-*b*-PCL$_{11}$ block copolymer, which predominantly comprised spherical micelles, was synthesized (Figure 4g, entry 3 in Table 1). When [PIB$_{50}$-OH]$_0$/[ε-CL]$_0$ was increased to 1/24, the PIB$_{50}$-*b*-PCL$_{27}$ diblock copolymer, which comprised fusiform and spherical micelles, was synthesized (Figure 4h,h′, entry 6 in Table 1). Finally, at [PIB$_{50}$-OH]$_0$/[ε-CL]$_0$ = 1/48, the PIB$_{50}$-*b*-PCL$_{49}$ diblock copolymer precipitated (entry 9 in Table 1).

The TEM images and corresponding DSC thermograms suggested that at the lowest polymerization temperature (20 °C), the PCL block was gradually generated and then crystallized because the polymerization temperature was below both T_m and T_c for the PCL block. The self-assembly of diblock copolymer was driven by the crystallization, and synthesized nanoparticles could be fixed *in situ*. At the highest polymerization temperature (80 °C), which was above both T_m and T_c for the PCL block, the PCL block melted and the morphology of nanoparticles could not be efficiently fixed.

https://doi.org/10.1021/acs.macromol.3c00681
Macromolecules 2023, 56, 4814−4822

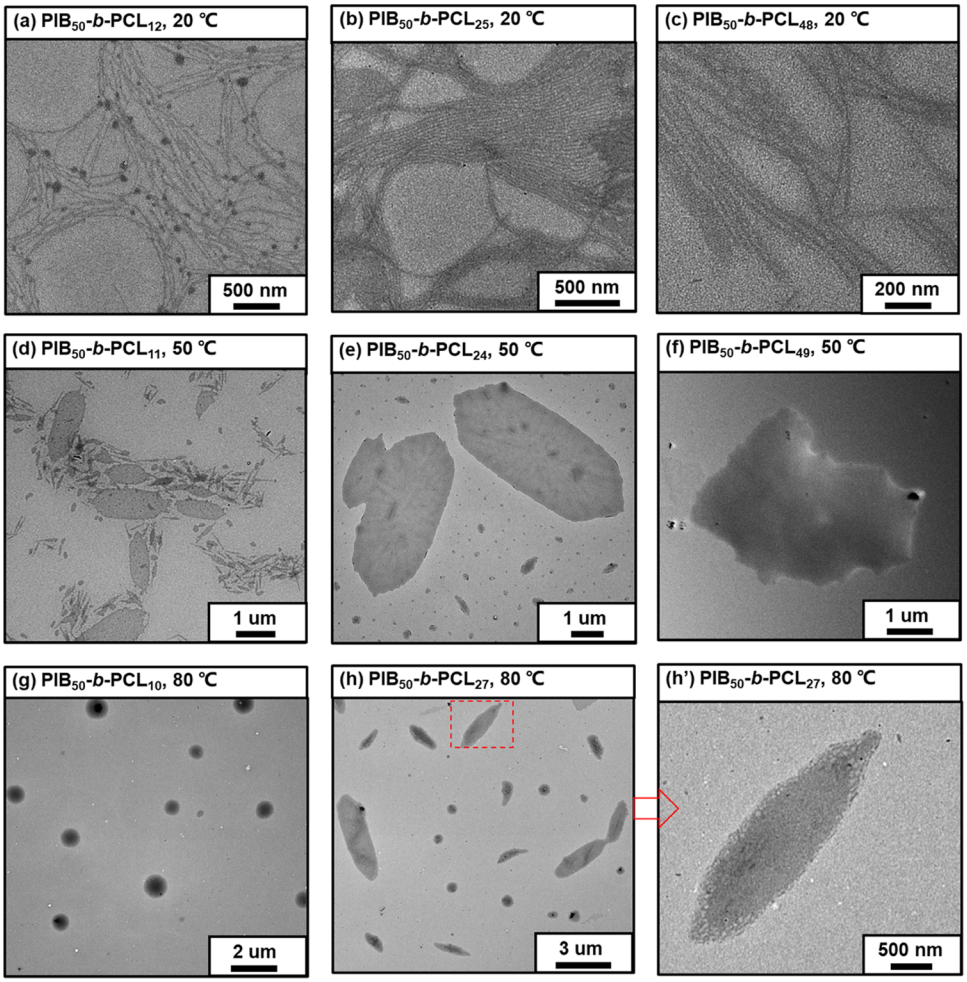

Figure 4. (a–h) TEM images of nanoparticles diluted in 0.05–0.1% w/w dispersion. Sample prepared using ROPISA on a copper grid was not stained. PIB_{50}-OH, ε-CL, and cyclohexane were the stabilizer/macroinitiator, monomer, and solvent, respectively. Solids were 10% w/w, and polymerization temperatures were 20, 50, and 80 °C.

However, when the ROPISA system was cooled to 20 °C, the block copolymer was reorganized and the morphology of nanoparticles could be fixed. During cooling, either spherical or fusiform micelles may form possibly owing to the stirring-generated shear. To confirm this hypothesis, ROPISA was performed under stirring at 500 rpm and 80 °C, and the stirring rate was subsequently changed during cooling. At a stirring rate of 0 rpm (*i.e.*, no stirring) during cooling, the block copolymer rapidly precipitated (entry 1 in Table S1). When the stirring rate was increased to 100, 500, and 1000 rpm during cooling, pure fusiform, a mixture of spherical and fusiform, and pure spherical micelles were formed, respectively (Figure S9, entries 2–4 in Table S1). Obviously, higher stirring rates should contribute to relatively stronger shears, which form spherical nanoparticles. In contrast, lower stirring rates (or weaker shears) generate precipitates or larger nanoparticles. Thus, for a parallel comparison, the stirring rate was fixed at 500 rpm for all of the ROPISA system. Alternatively, at a polymerization temperature of 50 °C, which is near both T_m and T_c for the PCL block, the diblock copolymer was semifused. When the diblock copolymer was cooled to 20 °C, short fibrillar and plate-like micelles were predominantly synthesized. These results suggested that the crystallization was indeed the predominant driving force for ROPISA, which could be alternatively modulated by changing the polymerization temperature. At different polymerization temperatures, nanoparticles were generated through distinct pathways.

Additionally, the morphologies of the nanoparticles generated using PIB-*b*-PVL diblock copolymers exhibiting different PVL lengths and synthesized at 20 °C were evaluated and compared. As shown in Figure S10 (entry 11 in Table 1), at $[PIB_{50}\text{-OH}]_0/[\delta\text{-VL}]_0$ = 1/12, the PIB_{50}-*b*-PVL_{10} diblock copolymer, which comprised fibrillar micelles and an irregular structure, was synthesized. However, at $[PIB_{50}\text{-OH}]_0/[\delta\text{-VL}]_0$ = 1/24 and 1/48, the diblock copolymer directly precipitated (entries 12 and 13 in Table 1). Compared with the nanoparticles synthesized using PIB_{50}-*b*-PCL_{25} and PIB_{50}-*b*-PCL_{48} containing core-forming blocks exhibiting similar DPs (entries 4 and 7 in Table 1), the nanoparticles synthesized using PIB_{50}-*b*-PVL_{24} and PIB_{50}-*b*-PVL_{46} were ready to precipitate. Although T_m and T_c for the PVL block were both near those for the PCL block (Figure 3c,d), the self-assembly ability of PIB-*b*-PVL was reduced because PVL is less soluble than PCL in cyclohexane.

Morphological Evolution of PIB-*b*-P(CL-*co*-VL) during ROPISA. For the PCL and PVL homopolymers, T_m and T_c were almost constant, which limited the nanoparticle morphological window at a certain temperature (20, 50, or 80 °C) owing to the defined crystallization ability and solubility of the core-forming block in cyclohexane. However,

https://doi.org/10.1021/acs.macromol.3c00681
Macromolecules 2023, 56, 4814–4822

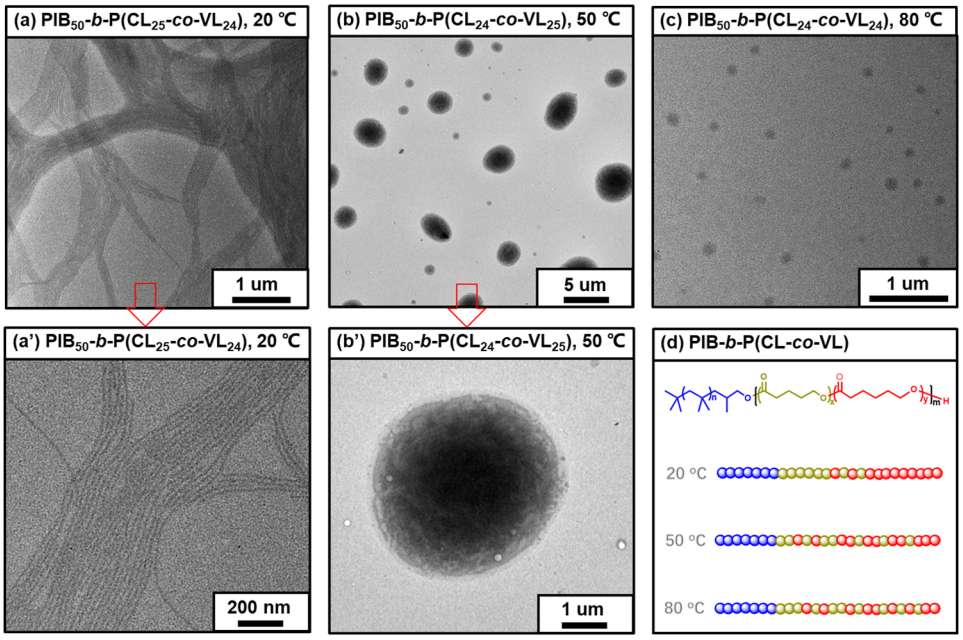

Figure 5. (a–c) TEM images of nanoparticles diluted in 0.05–0.2% w/w dispersion. Sample prepared using ROPISA on a copper grid was not stained. PIB_{50}-OH, ε-CL and δ-VL, and cyclohexane were the stabilizer/macroinitiator, comonomers, and solvent, respectively. Solids were 10% w/w, and polymerization temperatures were 20, 50, and 80 °C. (d) Schematic of PIB-*b*-P(CL-*co*-VL) copolymers with similar compositions and synthesized using ROPISA at different polymerization temperatures.

for the PIB-*b*-P(CL-*co*-VL) copolymers with similar compositions, the T_m and T_c, crystallization, and resulting ROPISA could be modulated by varying the sequences of ε-CL and δ-VL units, which were, in turn, affected by the polymerization temperature. Thus, a broader nanoparticle morphological range could be achieved, which enabled ROPISA to be controlled in a versatile manner.

As shown in Figure 5a,a′ (entry 14 in Table 1), at a polymerization temperature of 20 °C, the PIB_{50}-*b*-P(CL_{25}-*co*-VL_{24}) copolymer formed fibrillar micelles, and the PIB_{50}-*b*-P(CL_{25}-*co*-VL_{24}) copolymer functioned as a PIB_{50}-*b*-PVL_{24}-*b*-PCL_{25} triblock copolymer owing to the distinct polymerization rates of the ε-CL and δ-VL monomers. PIB_{50}-*b*-P(CL_{25}–*co*–VL_{24}) remained highly crystalline, which facilitated the formation of fibrillar micelles. Alternatively, at a polymerization temperature of 50 °C, the PIB-*b*-P(CL-*co*-VL) copolymer formed spherical micelles with a diameter of approx. 2200 nm (Figure 5b,b′, entry 15 in Table 1). However, at the highest polymerization temperature (80 °C), P(CL-*co*-VL) functioned more like a random copolymer and exhibited a relatively low crystallinity, which indicated that the solubility was the driving force for the self-assembly and facilitated the formation of spherical micelles with a diameter of approx. 110 nm (Figure 5c, entry 16 in Table 1). These results suggested that during ROPISA for the PIB-*b*-P(CL-*co*-VL) copolymer, the sequence of the ε-CL and δ-VL units played an important role on morphological evolution and that the monomer sequence could be conveniently modulated by adjusting the polymerization temperature (Figure 5d).

CONCLUSIONS

ROPISA was developed using biodegradable, biocompatible, and crystallizable polylactones (PCL, PVL, and P(CL-*co*-VL)) as core-forming blocks. The impact of the polymerization temperature (20, 50, and 80 °C) on the crystallization behavior and corresponding self-assembly of block copolymers was investigated. For PIB-*b*-PCL and PIB-*b*-PVL, spherical micelles or precipitates formed at the highest polymerization temperature (80 °C) and fibrillar micelles predominantly formed at the lowest polymerization temperature (20 °C), probably because of a different self-assembly route, which was dominated by crystallization. For PIB-*b*-P(CL-*co*-VL), the highest polymerization temperature (80 °C) led to the formation of P(CL-*co*-VL), which exhibited a random structure that resulted in the formation of spherical micelles. The lowest polymerization temperature (20 °C) facilitated the generation of P(CL-*co*-VL), which contained a quasi-block structure that led to the collection of fibrillar micelles. At different polymerization temperatures, nanoparticles with similar compositions exhibited different morphologies. This study provided an alternative method for modulating PISA. Moreover, the facile and versatile ROPISA technique provided a platform for developing a series of novel bio-based materials, which showed large-scale potential for industrial biorelevant applications.

ASSOCIATED CONTENT

Supporting Information

The Supporting Information is available free of charge at https://pubs.acs.org/doi/10.1021/acs.macromol.3c00681.

Experimental section; synthetic route for PIB_{50}-OH; GPC curves for HRPIB and PIB_{50}-OH; polymerization kinetics for ROPISA of ε-CL at 20, 50, and 80 °C; polymerization kinetics for ROPISA of δ-VL at 20 °C; polymerization kinetics for ROPISA of ε-CL and δ-VL at 20, 50, and 80 °C; data and TEM images of the nanoparticles formed in the ROPISA process employing the stirring rate of 500 rpm at 80 °C and different stirring rates during cooling to 20 °C; and TEM image of nanoparticles from PIB_{50}-*b*-PVL_{10} formed in the ROPISA process (PDF)

https://doi.org/10.1021/acs.macromol.3c00681
Macromolecules 2023, 56, 4814–4822

AUTHOR INFORMATION

Corresponding Author

Guowei Wang − *State Key Laboratory of Molecular Engineering of Polymers, Department of Macromolecular Science, Fudan University, Shanghai 200433, China;* orcid.org/0000-0003-2595-8269; Email: gwwang@fudan.edu.cn

Authors

Ding Shen − *State Key Laboratory of Molecular Engineering of Polymers, Department of Macromolecular Science, Fudan University, Shanghai 200433, China*

Boyang Shi − *State Key Laboratory of Molecular Engineering of Polymers, Department of Macromolecular Science, Fudan University, Shanghai 200433, China*

Peng Zhou − *State Key Laboratory of Molecular Engineering of Polymers, Department of Macromolecular Science, Fudan University, Shanghai 200433, China*

Di Li − *State Key Laboratory of Molecular Engineering of Polymers, Department of Macromolecular Science, Fudan University, Shanghai 200433, China;* orcid.org/0000-0001-9017-9582

Complete contact information is available at: https://pubs.acs.org/10.1021/acs.macromol.3c00681

Notes

The authors declare no competing financial interest.

ACKNOWLEDGMENTS

The authors thank the National Natural Science Foundation of China (21774022 and 22271058) for financial support.

REFERENCES

(1) Hu, S. Y.; Zhao, J. P.; Zhang, G. Z.; Schlaad, H. Macromolecular architectures through organocatalysis. *Prog. Polym. Sci.* **2017**, *74*, 34−77.

(2) Song, Q. L.; Hu, S. Y.; Zhao, J. P.; Zhang, G. Z. Organocatalytic copolymerization of mixed type monomers. *Chin. J. Polym. Sci.* **2017**, *35*, 581−601.

(3) Pietrangelo, A.; Knight, S. C.; Gupta, A. K.; Yao, L. J.; Hillmyer, M. A.; Tolman, W. B. Mechanistic Study of the Stereoselective Polymerization of D,L-Lactide Using Indium(III) Halides. *J. Am. Chem. Soc.* **2010**, *132*, 11649−11657.

(4) Schneiderman, D. K.; Hillmyer, M. A. Aliphatic Polyester Block Polymer Design. *Macromolecules* **2016**, *49*, 2419−2428.

(5) Watts, A.; Kurokawa, N.; Hillmyer, M. A. Strong, Resilient, and Sustainable Aliphatic Polyester Thermoplastic Elastomers. *Biomacromolecules* **2017**, *18*, 1845−1854.

(6) Hillmyer, M. A.; Tolman, W. B. Aliphatic Polyester Block Polymers: Renewable, Degradable, and Sustainable. *Acc. Chem. Res.* **2014**, *47*, 2390−2396.

(7) Batiste, D. C.; Meyersohn, M. S.; Watts, A.; Hillmyer, M. A. Efficient Polymerization of Methyl-epsilon-Caprolactone Mixtures To Access Sustainable Aliphatic Polyesters Derek. *Macromolecules* **2020**, *53*, 1795−1808.

(8) Makiguchi, K.; Satoh, T.; Kakuchi, T. Diphenyl Phosphate as an Efficient Cationic Organocatalyst for Controlled/Living Ring-Opening Polymerization of delta-Valerolactone and epsilon-Caprolactone. *Macromolecules* **2011**, *44*, 1999−2005.

(9) Makiguchi, K.; Ogasawara, Y.; Kikuchi, S.; Satoh, T.; Kakuchi, T. Diphenyl Phosphate as an Efficient Acidic Organocatalyst for Controlled/Living Ring-Opening Polymerization of Trimethylene Carbonates Leading to Block, End-Functionalized, and Macrocyclic Polycarbonates. *Macromolecules* **2013**, *46*, 1772−1782.

(10) Makiguchi, K.; Kikuchi, S.; Yanai, K.; Ogasawara, Y.; Sato, S.; Satoh, T.; Kakuchi, T. Diphenyl Phosphate/4-Dimethylaminopyridine as an Efficient Binary Organocatalyst System for Controlled/Living Ring-Opening Polymerization of L-Lactide Leading to Diblock and End-Functionalized Poly(L-lactide)s. *J. Polym. Sci., Part A: Polym. Chem.* **2014**, *52*, 1047−1054.

(11) Fu, J.; Luan, B.; Yu, X.; Cong, Y.; Li, J.; Pan, C. Y.; Han, Y. C.; Yang, Y. M.; Li, B. Y. Self-assembly of crystalline-coil diblock copolymer in solvents with varying selectivity: From spinodal-like aggregates to spheres, cylinders, and lamellae. *Macromolecules* **2004**, *37*, 976−986.

(12) Inam, M.; Cambridge, G.; Pitto-Barry, A.; Laker, Z. P. L.; Wilson, N. R.; Mathers, R. T.; Dove, A. P.; O'Reilly, R. K. 1D vs. 2D shape selectivity in the crystallization-driven self-assembly of polylactide block copolymers. *Chem. Sci.* **2017**, *8*, 4223−4230.

(13) Petzetakis, N.; Dove, A. P.; O'Reilly, R. K. Cylindrical micelles from the living crystallization-driven self-assembly of poly(lactide)-containing block copolymers. *Chem. Sci.* **2011**, *2*, 955−960.

(14) He, Y. X.; Eloi, J. C.; Harniman, R. L.; Richardson, R. M.; Whittell, G. R.; Mathers, R. T.; Dove, A. P.; O'Reilly, R. K.; Manners, I. Uniform Biodegradable Fiber-Like Micelles and Block Comicelles via "Living" Crystallization-Driven Self-Assembly of Poly(-lactide) Block Copolymers: The Importance of Reducing Unimer Self-Nucleation via Hydrogen Bond Disruption. *J. Am. Chem. Soc.* **2019**, *141*, 19088−19098.

(15) Du, Z. X.; Xu, J. T.; Fan, Z. Q. Micellar morphologies of poly(epsilon-caprolactone)-b-poly(ethylene oxide) block copolymers in water with a crystalline core. *Macromolecules* **2007**, *40*, 7633−7637.

(16) He, W. N.; Zhou, B.; Xu, J. T.; Du, B. Y.; Fan, Z. Q. Two Growth Modes of Semicrystalline Cylindrical Poly(epsilon-caprolactone)-b-poly(ethylene oxide) Micelles. *Macromolecules* **2012**, *45*, 9768−9778.

(17) Rizis, G.; van de Ven, T. G. M.; Eisenberg, A. "Raft" Formation by Two-Dimensional Self-Assembly of Block Copolymer Rod Micelles in Aqueous Solution. *Angew. Chem., Int. Ed.* **2014**, *53*, 9000−9003.

(18) Rizis, G.; van de Ven, T. G. M.; Eisenberg, A. Homopolymers as Structure-Driving Agents in Semicrystalline Block Copolymer Micelles. *ACS Nano* **2015**, *9*, 3627−3640.

(19) Lim Soo, P.; Luo, L. B.; Maysinger, D.; Eisenberg, A. Incorporation and release of hydrophobic probes in biocompatible polycaprolactone-block-poly(ethylene oxide) micelles: Implications for drug delivery. *Langmuir* **2002**, *18*, 9996−10004.

(20) Geng, Y.; Discher, D. E. Hydrolytic degradation of poly(ethylene oxide)-block-polycaprolactone worm micelles. *J. Am. Chem. Soc.* **2005**, *127*, 12780−12781.

(21) Geng, Y.; Dalhaimer, P.; Cai, S. S.; Tsai, R.; Tewari, M.; Minko, T.; Discher, D. E. Shape effects of filaments *versus* spherical particles in flow and drug delivery. *Nat. Nanotechnol.* **2007**, *2*, 249−255.

(22) Zhang, W. J.; Hong, C. Y.; Pan, C. Y. Polymerization-Induced Self-Assembly of Functionalized Block Copolymer Nanoparticles and Their Application in Drug Delivery. *Macromol. Rapid Commun.* **2019**, *40*, No. 1800279.

(23) Warren, N. J.; Armes, S. P. Polymerization-Induced Self-Assembly of Block Copolymer Nano-objects via RAFT Aqueous Dispersion Polymerization. *J. Am. Chem. Soc.* **2014**, *136*, 10174−10185.

(24) Canning, S. L.; Smith, G. N.; Armes, S. P. A Critical Appraisal of RAFT-Mediated Polymerization-Induced Self Assembly. *Macromolecules* **2016**, *49*, 1985−2001.

(25) Penfold, N. J. W.; Yeow, J.; Boyer, C.; Armes, S. P. Emerging Trends in Polymerization-Induced Self-Assembly. *ACS Macro Lett.* **2019**, *8*, 1029−1054.

(26) Lv, F.; An, Z. S.; Wu, P. Y. Scalable preparation of alternating block copolymer particles with inverse bicontinuous mesophases. *Nat. Commun.* **2019**, *10*, No. 1379.

(27) Shi, B. Y.; Shen, D.; Li, W.; Wang, G. W. Self-Assembly of Copolymers Containing Crystallizable Blocks: Strategies and Applications. *Macromol. Rapid Commun.* **2022**, *43*, No. 202200071.

(28) Wan, J.; Fan, B.; Thang, S. H. RAFT-mediated polymerization-induced self-assembly (RAFT-PISA): current status and future directions. *Chem. Sci.* **2022**, *13*, 4192−4224.
(29) Wang, J.; Cao, M. Y.; Zhou, P.; Wang, G. W. Exploration of a Living Anionic Polymerization Mechanism into Polymerization-Induced Self-Assembly and Site-Specific Stabilization of the Formed Nano-Objects. *Macromolecules* **2020**, *53*, 3157−3165.
(30) Derry, M. J.; Fielding, L. A.; Armes, S. P. Polymerization-induced self-assembly of block copolymer nanoparticles via RAFT non-aqueous dispersion polymerization. *Prog. Polym. Sci.* **2016**, *52*, 1−18.
(31) Shi, B. Y.; Wang, G. W. Application of Polymerization-induced Self-assembly (PISA) Technology. *Acta Polym. Sin.* **2022**, *53*, 15−29.
(32) Niu, B.; Chen, Y.; Zhang, L.; Tan, J. B. Organic-inorganic hybrid nanomaterials prepared via polymerization-induced self-assembly: recent developments and future opportunities. *Polym. Chem.* **2022**, *13*, 2554−2569.
(33) Kuperkar, K.; Patel, D.; Atanase, L. I.; Bahadur, P. Amphiphilic Block Copolymers: Their Structures, and Self-Assembly to Polymeric Micelles and Polymersomes as Drug Delivery Vehicles. *Polymers* **2022**, *14*, No. 4702.
(34) Qiu, L.; Han, X. Y.; Xing, C. F.; Glebe, U. Polymerization-Induced Self-Assembly: An Emerging Tool for Generating Polymer-Based Biohybrid Nanostructures. *Small* **2023**, *19*, No. 202207457.
(35) Boott, C. E.; Gwyther, J.; Harniman, R. L.; Hayward, D. W.; Manners, I. Scalable and uniform 1D nanoparticles by synchronous polymerization, crystallization and self-assembly. *Nat. Chem.* **2017**, *9*, 785−792.
(36) Oliver, A. M.; Gwyther, J.; Boott, C. E.; Davis, S.; Pearce, S.; Manners, I. Scalable Fiber-like Micelles and Block Co-micelles by Polymerization-Induced Crystallization-Driven Self-Assembly. *J. Am. Chem. Soc.* **2018**, *140*, 18104−18114.
(37) Hurst, P. J.; Rakowshi, A. M.; Patterson, J. P. Ring-opening polymerization-induced crystallization-driven self-assembly of poly-L-lactide-block-polyethylene glycol block copolymers (ROPI-CDSA). *Nat.Commun.* **2020**, *11*, No. 4690.
(38) Jiang, J. H.; Zhang, X. Y.; Fan, Z.; Du, J. Z. Ring-Opening Polymerization of N-Carboxyanhydride-Induced Self-Assembly for Fabricating Biodegradable Polymer Vesicles. *ACS Macro Lett.* **2019**, *8*, 1216−1221.
(39) Grazon, C.; Salas-Ambrosio, P.; Ibarboure, E.; Buol, A.; Garanger, E.; Grinstaff, M. W.; Lecommandoux, S.; Bonduelle, C. Aqueous Ring-Opening Polymerization Induced Self-Assembly (ROPISA) of N-carboxyanhydrides. *Angew. Chem., Int. Ed.* **2020**, *59*, 622−626.
(40) Grazon, C.; Salas-Ambrosio, P.; Antoine, S.; Ibarboure, E.; Sandre, O.; Clulow, A. J.; Boyd, B.; Grinstaff, M. W.; Lecommandoux, S.; Bonduelle, C. Aqueous ROPISA of alpha-amino acid N-carboxyanhydrides: polypeptide block secondary structure controls nanoparticle shape anisotropy. *Polym. Chem.* **2021**, *12*, 6242−6251.
(41) Shi, Q. Q.; Chen, Y. B.; Yang, J. J.; Yang, J. Ring-opening polymerization-induced self-assembly (ROPISA) of salicylic acid o-carboxyanhydride. *Chem. Commun.* **2021**, *57*, 11390−11393.
(42) Ellis, C. E.; Garcia-Hernandez, J. D.; Manners, I. Scalable and Uniform Length-Tunable Biodegradable Block Copolymer Nanofibers with a Polycarbonate Core via Living Polymerization-Induced Crystallization-Driven Self-assembly. *J. Am. Chem. Soc.* **2022**, *144*, 20525−20538.
(43) Jiang, J. H.; Zhu, Y. Q.; Du, J. Z. Challenges and Perspective on Ring-Opening Polymerization-Induced Self-Assembly. *Acta Chim. Sin.* **2020**, *78*, 719−724.
(44) Kostjuk, S. V.; Yeong, H. Y.; Voit, B. Cationic Polymerization of Isobutylene at Room Temperature. *J. Polym. Sci., Part A: Polym. Chem.* **2013**, *51*, 471−486.
(45) Singh, A. K.; Singh, R. K. A Search for Ecofriendly Detergent/Dispersant Additives for Vegetable-Oil Based Lubricants. *J. Surfactants Deterg.* **2012**, *15*, 399−409.
(46) Wang, S. P.; Yu, S. S.; Feng, J. X.; Liu, S. G. Multifunctional lubricant additive derived from polyisobutylene succinimide dispersant. *J. Dispersion Sci. Technol.* **2021**, *42*, 396−406.
(47) Tsunogae, Y.; Kennedy, J. P. Living Carbocationic Polymerization. 58. Polyisobutylene-Containing Block Polymers by Sequential Monomer Addition. 10. Synthesis of Poly(Alpha-Methylstyrene-B-Isobutylene-B-Alpha-Methylstyrene) Thermoplastic Elastomers. *J. Polym. Sci., Part A: Polym. Chem.* **1994**, *32*, 403−412.
(48) Kennedy, J. P.; Midha, S.; Tsunogae, Y. Living Carbocationic Polymerization. 56. Polyisobutylene-Containing Block Polymers by Sequential Monomer Addition. 8. Synthesis, Characterization, and Physical-Properties of Poly(Indene-B-Isobutylene-B-Indene) Thermoplastic Elastomers. *Macromolecules* **1993**, *26*, 429−435.
(49) Nasrollahzadeh, M.; Ganji, F.; Taghizadeh, S. M.; Vasheghani-Farahani, E. ″D-optimal experimental design″ analysis in preparing optimal polyisobutylene based pressure sensitive adhesives. *Int. J. Adhes. Adhes.* **2017**, *78*, 28−37.
(50) Kekec, N. C.; Akolpoglu, M. B.; Bozuyuk, U.; Kizilel, S.; Nugay, N.; Nugay, T.; Kennedy, J. P. Calcification resistance of polyisobutylene and polyisobutylene-based materials. *Polym. Adv. Technol.* **2019**, *30*, 1836−1846.
(51) Zhou, Y. H.; Faust, R.; Richard, R.; Schwarz, M. Syntheses and characterization of poly(cyclohexyl vinyl ether-stat-vinyl alcohol)-b-polyisobutylene-b-poly(cyclohexyl vinyl ether-stat-vinyl alcohol) triblock copolymers and their application as coatings to deliver paclitaxel from coronary stents. *Macromolecules* **2005**, *38*, 8183−8191.
(52) El Fray, M.; Prowans, P.; Puskas, J. E.; Altstadt, V. Biocompatibility and fatigue properties of polystyrene-polyisobutylene-polystyrene, an emerging thermoplastic elastomeric biomaterial. *Biomacromolecules* **2006**, *7*, 844−850.
(53) Ojha, U.; Kulkarni, P.; Faust, R. Syntheses and characterization of novel biostable polyisobutylene based thermoplastic polyurethanes. *Polymer* **2009**, *50*, 3448−3457.
(54) Lim, G. T.; Puskas, J. E.; Reneker, D. H.; Jakli, A.; Horton, W. E. Highly Hydrophobic Electrospun Fiber Mats from Polyisobutylene-Based Thermoplastic Elastomers. *Biomacromolecules* **2011**, *12*, 1795−1799.
(55) Ren, K.; Zhang, M. Z.; He, J. L.; Wu, Y. X.; Ni, P. H. Preparation of Polymeric Prodrug Paclitaxel-Poly(lactic acid)-b-Polyisobutylene and Its Application in Coatings of a Drug Eluting Stent. *ACS Appl. Mater. Interfaces* **2015**, *7*, 11263−11271.
(56) Wu, Y. B.; Li, K.; Xiang, D.; Zhang, M.; Yang, D.; Zhang, J. H.; Mao, J.; Wang, H.; Guo, W. L. Surface immobilization of heparin on functional polyisobutylene-based thermoplastic elastomer as a potential artificial vascular graft. *Appl. Surf. Sci.* **2018**, *445*, 8−15.
(57) Liu, Q. A.; Wu, Y. X.; Yan, P. F.; Zhang, Y.; Xu, R. W. Polyisobutylene with High exo-Olefin Content via beta-H Elimination in the Cationic Polymerization of Isobutylene with H2O/FeCl3/Dialkyl Ether Initiating System. *Macromolecules* **2011**, *44*, 1866−1875.
(58) Vasilenko, I. V.; Kostjuk, S. V. Homogeneous and heterogeneous catalysts for the synthesis of highly reactive polyisobutylene: discovery, development and perspectives. *J. Macromol. Sci. A* **2021**, *58*, 725−735.
(59) Dejuana, R.; Cortazar, M. Study of the Melting and Crystallization Behavior of Binary Poly(Epsilon-Caprolactone) Poly(Hydroxy Ether of Bisphenol-a) Blends. *Macromolecules* **1993**, *26*, 1170−1176.
(60) Bogdanov, B.; Vidts, A.; Schacht, E.; Berghmans, H. Isothermal crystallization of poly(epsilon-caprolactone-ethylene glycol) block copolymers. *Macromolecules* **1999**, *32*, 726−731.
(61) Mishra, G. P.; Kinser, R.; Wierzbicki, I. H.; Alany, R. G.; Alani, A. W. G. In situ gelling polyvalerolactone-based thermosensitive hydrogel for sustained drug delivery. *Eur. J. Pharm. Biopharm.* **2014**, *88*, 397−405.
(62) Jutier, J. J.; Lemieux, E.; Prudhomme, R. E. Miscibility of Polyester Nitrocellulose Blends - a Dsc and Ftir Study. *J. Polym. Sci., Part B: Polym. Phys.* **1988**, *26*, 1313−1329.

https://doi.org/10.1021/acs.macromol.3c00681
Macromolecules 2023, 56, 4814−4822